

Discovery of Charge Density Waves in Cuprate Superconductors

up to the Critical Doping and Beyond

H. Miao^{1*}, G. Fabbris², R. Koch¹, D. G. Mazzone¹, C. S. Nelson³, R. Acevedo-Esteves³,
Y. Li¹, G. D. Gu¹, T. Yilmaz³, K. Kaznatcheev³, E. Vescovo³, M. Oda⁴, T. Kurosawa⁴, N.
Momono⁵, T. A. Assefa¹, I. K. Robinson^{1,6}, E. Bozin¹, J. M. Tranquada¹, P. D. Johnson¹
and M. P. M. Dean^{1*}

¹*Condensed Matter Physics and Materials Science Department, Brookhaven National
Laboratory, Upton, New York 11973, USA*

²*Advanced Photon Source, Argonne National Laboratory, Argonne, Illinois 60439, USA*

³*National Synchrotron Light Source II, Brookhaven National Laboratory, Upton, New
York, 11973, USA*

⁴*Department of Physics, Hokkaido University, Sapporo 060-0810, Japan*

⁵*Department of Sciences and Informatics, Muroran Institute of Technology, Muroran
050-8585, Japan*

⁶*London Centre for Nanotechnology, University College, Gower St., London WC1E
6BT, UK.*

**To whom correspondence should be addressed. E-mail : hmiao@bnl.gov ;
mdean@bnl.gov.*

**The unconventional normal-state properties of the cuprates are often discussed in
terms of emergent electronic order that onsets below a putative critical doping,
 $x_c \approx 0.19$. Charge density wave (CDW) correlations represent one such order;
however, experimental evidence for such order generally spans a limited range of**

doping that falls short of the critical value x_c , leading to questions regarding its essential relevance. Here, we use x-ray diffraction to demonstrate that CDW correlations in $\text{La}_{2-x}\text{Sr}_x\text{CuO}_4$ persist up to a doping of at least $x = 0.21$. The correlations show strong changes through the superconducting transition, but no obvious discontinuity through $x_c \approx 0.19$, despite changes in Fermi surface topology and electronic transport at this doping. These results prompt a reconsideration of the role of CDW correlations in the high- T_c cuprate phase diagram.

The cuprate high- T_c superconductors are often conceptualized as doped Mott insulators, in which the electronic ground state spontaneously breaks rotational and/or translational symmetry^{1,2}. While cuprate CDW correlations were discovered over two decades ago³, their possible contribution to the cuprates' anomalous electronic properties remains a matter of vigorous debate^{1,4-8} with increasing attention in light of the ubiquity of CDW order in different cuprate families^{3,9-17}. The cuprate phase diagram, shown in Fig. 1A, shows that pseudogap, strange metal, and superconducting phases exist over an extensive doping range below a critical doping level of $x_c \approx 0.19$, above which the cuprate electronic properties become gradually more Fermi-liquid-like¹⁸⁻²⁵. If CDW correlations are confined only to the underdoped cuprates, as previous studies suggested⁹⁻¹⁶, that would preclude the possibility of CDW correlations having an important role in the anomalous electronic properties. It has, for example, been argued that since CDW correlations disappear at $x \ll x_c$, the nominal quantum critical point (QCP) associated

with the termination of pseudogap must be magnetic in nature⁶. Alternatively, recent tunneling spectroscopy studies have suggested a vestigial nematic QCP^{26,27}. The presence or absence of CDW correlations is also crucial for the relevance of intertwined order, as some theoretical models for pair density wave superconductors require the presence of CDW correlations^{1,28}. Recent x-ray measurements have observed CDW correlations in underdoped and optimally doped cuprates up to temperatures well above the nominal CDW transition temperature^{29,30}. This motivates proposals for phase diagrams in which CDW correlations extend up to higher dopings than previously thought³⁰. Herein, we address this issue by focusing on $\text{La}_{2-x}\text{Sr}_x\text{CuO}_4$ (LSCO_x) in view of its particularly well characterized transport properties and the feasibility of synthesizing high-quality samples across the whole phase diagram^{19,22-25}.

We start by illustrating the cuprate electronic structure evolution with doping as shown in Fig. 1B. At low doping, to the extent that a Fermi surface (FS) exists, it is hole-like and centered at the Brillouin zone (BZ) corner. Increasing the hole concentration decreases the chemical potential, which eventually passes through a saddle point of the Fermi surface at a doping close to x_c , resulting in a Lifshitz transition to an electron-like FS at the BZ center. Figure 1C-E shows angle-resolved photoemission spectroscopy (ARPES) measurements for LSCO₁₂, LSCO₁₇, and LSCO₂₁. The Lifshitz transition is seen between LSCO₁₇ and LSCO₂₁, consistent with $x_c = 0.19$ and with previous ARPES studies^{31,32}.

Having confirmed the electronic structure, we now show our main experimental finding of CDW correlations beyond x_c . Figure 2 plots x-ray reciprocal space scans for LSCO21 at $T = 16$ K, where reciprocal space is defined in terms of scattering vector $\mathbf{Q} = (H, K, L)$ using lattice constants $a = b \approx 3.8$ Å and $c \approx 13.2$ Å. High sensitivity is achieved by exploiting the high brightness of the National Synchrotron Light Source II and by careful configuration of the detection system to suppress background signal³³. Superlattice peaks are observed at (0.235, 0, 12.5), and equivalent locations, along both the H and K directions (Fig. 2 A and B). The observed $H = 0.235$ is essentially the same as the CDW wavevector in underdoped LSCO^{14-16,34} and is consistent with the charge stripe picture^{2,3}. The peaks are symmetric with respect to $\pm H$ and K and are observed in multiple Brillouin zones including ($\pm 0.235, 0, L$) for $L = 8.5$ & 12.5. An L -scan along $\mathbf{Q} = (-0.235, 0, L)$ (Fig. 2D) shows that the intensity is broadly peaked at half-integer L similar to underdoped LSCO¹⁴⁻¹⁶. These results demonstrate the presence of CDW correlations beyond x_c in LSCO.

Figure 3 summarizes the doping and temperature dependence of the CDW correlations. In Fig. 3A, Lorentzian-squared fits to the data are shown, which are parameterized in terms of amplitude, $I_{\text{CDW}}(T)$, and in-plane correlation length, $\xi_{||}(T) = 1 / \text{HWHM}$ (where HWHM is half-width at half-maximum). Since domain formation can lead to transverse peak splitting in LSCO (Refs. 14,34 and Fig. 3A), we scan through peaks in all three reciprocal space directions and use two Lorentzian-squared functions displaced in the K (transverse) direction where necessary to account for the full intensity distribution. Peak

widths are determined by the H (longitudinal) cut. $I_{\text{CDW}}(T)$ is found to be largest near T_{SC} for all dopings (Fig. 3B). Above T_{SC} , both I_{CDW} and $\xi_{\parallel}(T)$ decrease with increasing temperature but remain finite at least to $T = 90$ K (Fig. 3A). Interestingly, the correlation length can be separated into a nearly T -independent region where $\xi_{\parallel}(T)$ is approximately 4-unit-cells (about one period of the CDW order), and a strongly T -dependent region where $\xi_{\parallel}(T)$ continues to expand until SC intervenes. We refer to the CDW in the T -independent region as “precursor” CDW correlations in that they come before the emergence of a stronger, better-correlated CDW at low temperatures. (Note that for these measurements we do not have the energy resolution to directly distinguish between dynamic and static correlations.) This phenomenology is consistent with recent resonant inelastic x-ray scattering studies of $\text{La}_{2-x}\text{Ba}_x\text{CuO}_4$ (LBCO x) and $\text{YBa}_2\text{Cu}_3\text{O}_{6+\delta}$, which show a similar two-stage CDW formation^{29,30,35,36}. While the CDW evolves smoothly from LSCO12 to LSCO21, both ξ_{\parallel} and the onset temperature of the longer-range CDW, T_{ξ} , are suppressed in the overdoped regime around x_c (Fig.3C and Fig.4). No CDW correlations are observed in our high-sensitivity x-ray measurements at $x = 0.25$.

Previous measurements of the same $x = 0.12$ sample allow us to compare the CDW order parameter, taken to be captured by the total Q -integrated scattering intensity, to other cuprate systems¹⁴. The CDW order parameter of LSCO12 is only four times weaker than $\text{La}_{1.875}\text{Ba}_{0.125}\text{CuO}_4$ (which has the strongest zero-field CDW order). With increasing doping, the LSCO CDW becomes somewhat stronger for $x = 0.17$ and drops appreciably

for $x = 0.21^{33}$. Consequently, CDW correlations can have an appreciable effect on the physics of LSCO_x for dopings through x_c .

Figure 4 summarizes our main observations -- that CDW correlations exist across almost the whole doping phase diagram. It immediately yields two important consequences for the cuprates. Firstly, the very similar CDW properties that are observed either side of the Lifshitz transition, provide a vivid demonstration of the fact that they cannot be explained with a weak coupling Fermi surface nesting picture. Instead, the nearly constant \mathbf{Q}_{CDW} for doping $x > 0.125$ support strong coupling mechanisms, where the CDW is driven by a subtle balance between Coulomb interactions and kinetic energy². Secondly, the continuous evolution of the CDW correlations appear to be inconsistent with a QCP associated with CDW or coupled CDW/SDW order^{4,8}.

Our observations also urge a re-examination of the potential role of the CDW in the anomalous electronic properties of the cuprates. CDW correlations are a prerequisite (but not a proof) of several prominent theories of cuprate properties, which would be expected to apply across the phase diagram and not just in the underdoped cuprates where CDW correlations have been studied extensively in the past. These include the possibility that CDW correlations play a key role in the electronic transport properties^{4,8}. Theories of pair density wave order^{1,28,37,38}, which predict the type of competition between the CDW and uniform d-wave superconductivity, also fall in this category. As shown in Fig.3, both the CDW peak intensity and the CDW correlation length grow on cooling before saturating

below T_{SC} , without any clear evidence for a phase transition. This behavior would be consistent with a possible fluctuating CDW component that competes with superconductivity and could consequently affect cuprate transport properties^{22-25,30}.

Finally, we note that a charge Bragg peak has recently been observed in overdoped $(\text{Bi},\text{Pb})_{2.12}\text{Sr}_{1.88}\text{CuO}_{6+\delta}$ (Bi2201), with a maximum doping comparable to that observed here¹⁷. This state, termed re-entrant charge order, has several properties that are different to CDW states in LSCO and other cuprates. Re-entrant charge order appears to exist in an isolated region of the overdoped phase diagram, disconnected from the underdoped CDW order. The correlation length and temperature scale of the state are also far higher than other cuprates. Intriguingly, no interaction between the CDW and superconductivity is observed. All other similarly well-correlated CDW states are associated with strong suppression of superconducting order. All these behaviors are in strong contrast with the CDW in overdoped LSCO, where the CDW wavevectors, correlation length and temperature dependence evolve smoothly from the underdoped LSCO properties and strongly intertwine with low-temperature transport properties. Based on the electronic structure of Bi2201 and the wavevector of re-entrant charge order around 0.1 r.l.u., which extrapolates roughly linearly from the underdoped CDW wavevector, re-entrant charge order was proposed to arise due to a van Hove singularity¹⁷. The overdoped CDW in LSCO appears to have no connection to this mechanism. Instead, our observations support the strong coupling mechanisms, where the CDW is driven by a subtle balance between Coulomb interactions and kinetic energy².

In summary, high-sensitivity x-ray measurements have revealed that cuprate CDW correlations persist across almost the whole cuprate doping phase diagram, despite dramatic changes in the cuprate transport properties and Fermi surface topology, before disappearing when fermi-liquid-like properties are restored. We have shown that these correlations impact superconductivity even in overdoped cuprates, suggesting that CDW correlations can have a far more extensive role in the cuprate phase diagram than was previously envisaged, and prompting investigations of CDW correlations in other overdoped cuprates.

References and notes:

1. E. Fradkin, S. Kivelson and J. M. Tranquada, Rev. Mod. Phys. 87, 457 (2015).
2. V. J. Emery, S. A. Kivelson, H. Q. Lin, Phys. Rev. Lett. 64, 475 (1990).
3. J. M. Tranquada et al., Nature 375, 561 (1995).
4. C. Castellani, C. Di Castro and M. Grilli, Phys. Rev. Lett. 75, 4650 (1995).
5. S. Sachdev, Physica Status Solidi B 247, 537 (2010).
6. N. Doiron-Leyraud, and L. Taillefer, Physica C 481, 161 (2012).
7. S. E. Sebastian and C. Proust, Annu. Rev. Condens. Matter Phys. 6, 411 (2015).
8. S. Caprara, C. Di Castro, G. Seibold and M. Grilli, Phys. Rev. B 95, 224511 (2017).
9. J. E. Hoffman et al., Science 295, 466 (2002).
10. C. Howald, H. Eisaki, N. Kaneko and A. Kapitulnik, Proc. Natl. Acad. Sci. USA 100, 9705 (2003).
11. G. Ghiringhelli et al., Science 337, 821 (2012).

12. R. Comin et al., *Science* 343, 390 (2014).
13. W. Tabbis et al., *Nat. Commun.* 5, 5875 (2014).
14. V. Thampy et al., *Phys. Rev. B* 90, 100510 (2014).
15. T. P. Croft et al., *Phys. Rev. B* 89, 224513 (2014).
16. N. B. Christensen et al., *arXiv:1404.3192* (2014).
17. Y. Y. Peng et al., *Nature Materials* 17, 697 (2018).
18. Y. Wang, L. Li and N. P. Ong, *Phys. Rev. B* 73, 024510 (2006).
19. R. A. Cooper et al., *Science* 323, 603 (2009).
20. B. Keimer et al., *Nature* 518, 179–186 (2015)
21. B. Ramshaw et al., *Science* 348, 317-320 (2015).
22. S. Badoux et al., *Phys. Rev. X* 6, 021004 (2016).
23. P. Giraldo-Gallo et al., *Science* 361, 479 (2018).
24. G. S. Boebinger et al., *Phys. Rev. Lett.* 77, 5417 (1996).
25. B. Michon et al., *Nature* 567, 218–222 (2019).
26. L. Nie, G. Tarjus and S. A. Kivelson, *Proc. Natl. Acad. Sci. USA* 111, 7980 (2014).
27. S. Mukhopadhyay et al., *Proc. Natl. Acad. Sci. USA* 116, 13249-13254 (2019).
28. D. F. Agterberg et al., *arXiv: 1904.09687* (2019) *Annu. Rev. Condens. Matter Phys.* (in press).
29. H. Miao et al., *Proc. Natl. Acad. Sci. USA* 114, 12430 (2017).
30. R. Arpaia et al., *Science* 365, 906 (2019).
31. T. Yoshida et al., *Phys. Rev. B* 74, 224510 (2006).
32. M. Horio et al., *Phys. Rev. Lett.* 121, 077004 (2018).

33. Supplementary materials.
34. J. J. Wen et al., *Nat. Commun.* **10**, 3269 (2019).
35. H. Miao et al., *Phys. Rev. X* **8**, 011008 (2018).
36. H. Miao et al., *Phys. Rev. X* **9**, 031042 (2019).
37. P. A. Lee, *Phys. Rev. X* **4**, 031017 (2014).
38. E. Berg et al., *Phys. Rev. Lett.* **99**, 127003 (2007).
39. K. Yamada et al., *Phys. Rev. B* **57**, 6165 (1998).

Acknowledgements

We thank N. Christensen, G. Kotliar, J. Q. Lin, S. Kivelson, V. Thamby, A. Tsvelik and W. G. Yin for insightful discussions, and J. Jiang and S. S. Zhang for technical support.

Funding: This material is based upon work supported by the U.S. Department of Energy (DOE), Office of Basic Energy Sciences, Early Career Award Program under Award No. 1047478. Work at Brookhaven National Laboratory was supported by the U.S. Department of Energy, Office of Basic Energy Sciences, under Contract No. DESC0012704. X-ray and photoemission measurements used resources at the 4-ID and 21-ID-1 beamlines of the National Synchrotron Light Source II, a U.S. Department of Energy Office of Science User Facility operated for the DOE Office of Science by Brookhaven National Laboratory under Contract no. DE-SC0012704. Additional x-ray measurements used resources at 4-ID-D in the Advanced Photon Source, a U.S. Department of Energy (DOE) Office of Science User Facility operated for the DOE Office of Science by Argonne National Laboratory under Contract No. DE-AC02-06CH11357.

Author contribution: H.M., T.Y., K.K., E.V., and P.D.J. performed the ARPES measurement. H.M., G.F. T.A.A., I.K.R., R. A.-E, C.N., and M.P.M.D performed the x-ray measurements. Y.L., G.D.G., M.O., K.K., and N.M. grew the LSCO samples and characterized their transport properties. H.M., P.D.J., and M.P.M.D. analyzed the data. H.M., J.M.T., and M.P.M.D. wrote the paper. **Competing interests:** Authors declare no competing interests. **Data availability:** Data needed to evaluate the conclusions of this manuscript are presented in the main text and supplementary materials.

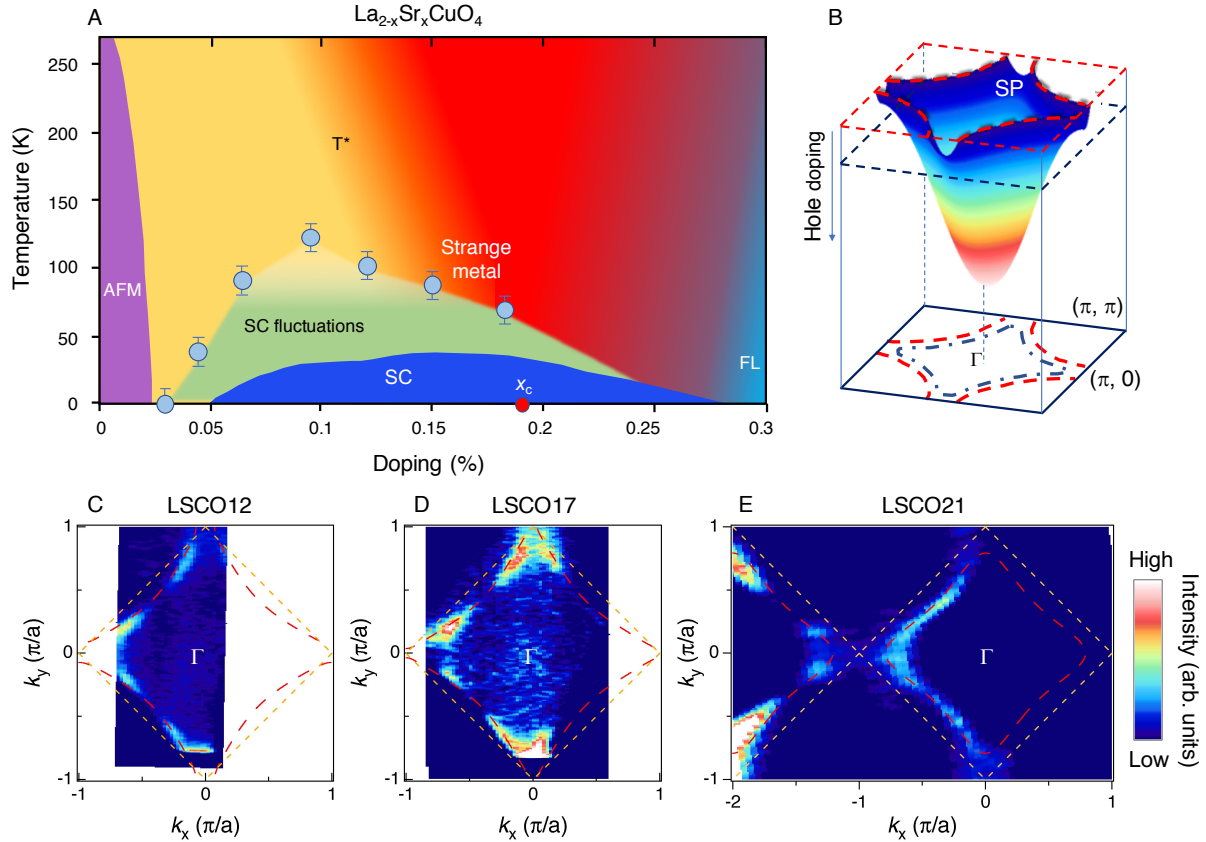


Figure 1: Doping dependent electronic structure of LSCO. (A) Phase diagram of the hole doped cuprates, constructed from magnetization, Nernst effect and resistivity data

for LSCO^{6,18}. (B) Schematic band structure of LSCO. The Fermi energy, E_F , crosses the anti-nodal saddle point (SP) near $x_c \approx 0.19$ driving a Lifshitz transition. (C)-(E) Fermi surface topology of LSCO12, LSCO17 and LSCO21. The intensity plots are obtained by integrating the spectra within ± 10 meV of E_F . Orange dashes outline the antiferromagnetic Brillouin zone. Red dashed contours represent a tight-binding fit of the FS. The data shown in (C)-(E) were collected at 11 K.

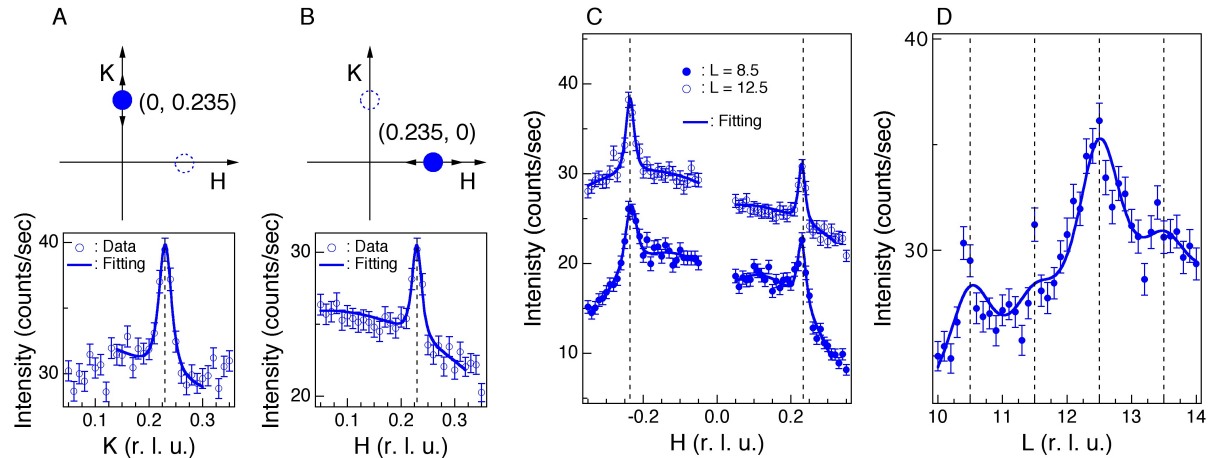


Figure 2: Discovery of a CDW beyond x_c in LSCO. (A) and (B) x-ray diffraction measurements of LSCO21 at $T = 16$ K along $(0, K, 12.5)$ and $(H, 0, 12.5)$. Peaks are observed at $(0, 0.235, 12.5)$ and $(0.235, 0, 12.5)$. The H-scans in (C) reveal further CDW peaks at $(\pm 0.235, 0, L)$ for $L = 8.5$ and 12.5 . The data at $L = 8.5$ are offset by -10 counts/second for visibility. (D) The L -dependence of the intensity along $(-0.235, 0, L)$ demonstrates poorly correlated out-of-phase CDW stacking along the c-axis. Solid curves in (A)-(D) are fits to the experimental data.

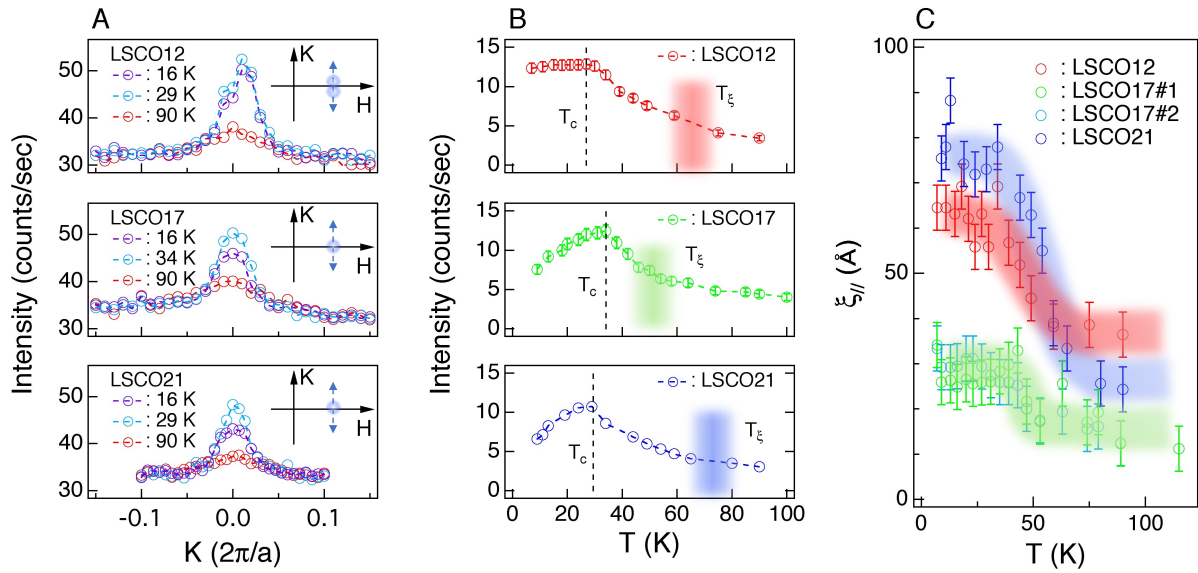


Figure 3: CDW temperature dependence. (A) Doping dependence of the CDW intensity for temperatures $T < T_{SC}$, $T \approx T_{SC}$, and $T > T_{SC}$. The inset of each panel represents the respective cut in reciprocal space. The intensity comparison of different samples was achieved via sequential measurements under similar conditions. (B) The temperature dependence of the CDW intensity in LSCO. The shaded area corresponds to T_ξ where the in-plane CDW correlation length, $\xi_{||}$, starts to increase, as determined in (C). The colored shaded curves in (C) track the temperature dependent $\xi_{||}$ for different dopings. The $\xi_{||}$ increases with decreasing temperature for $T_{SC} < T < T_\xi$. Two independent measurements of LSCO17 samples at different beamlines show consistent suppression of $\xi_{||}$ and T_ξ , indicating that systematic errors are minimal.

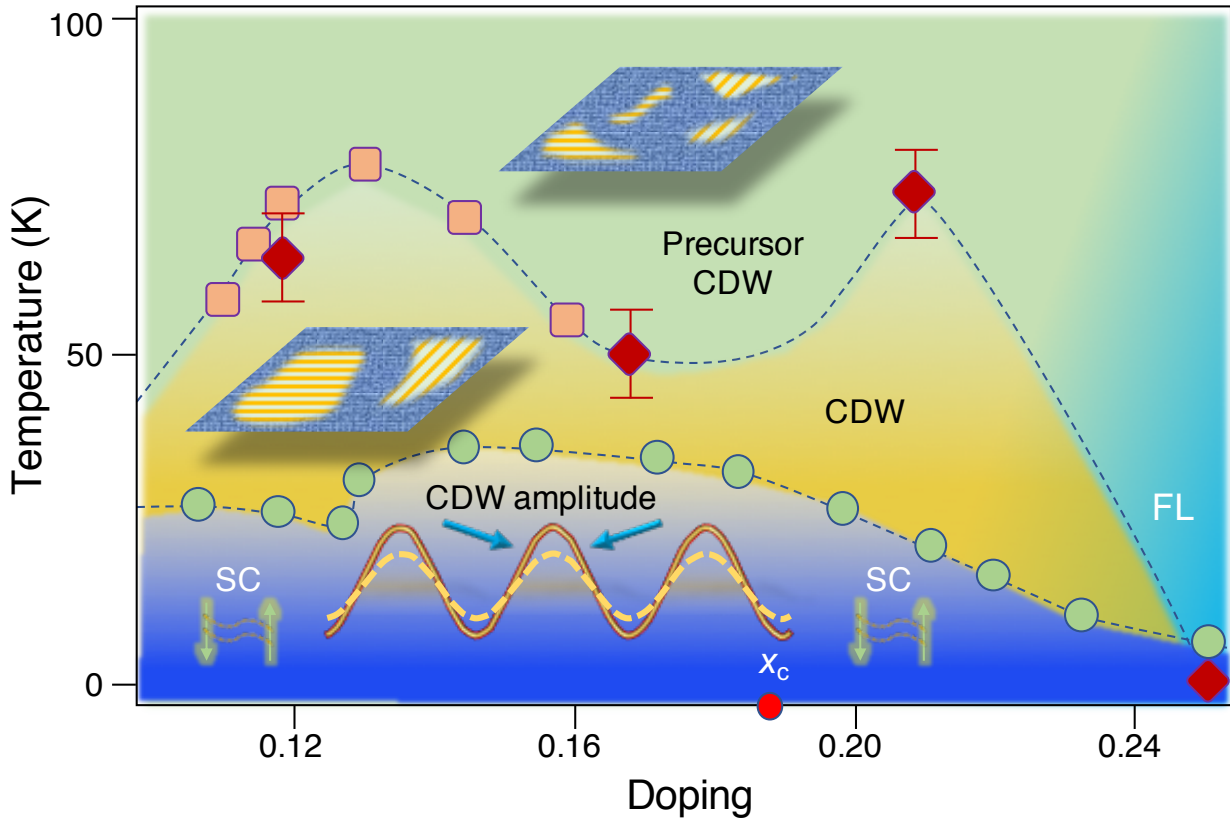


Figure 4: Illustration of the extent of CDW correlations in the cuprate phase diagram suggested by this work. Very short-range CDW correlations appear at high temperature for $0.12 < x < 0.21$, which we refer to as a precursor CDW^{29,35,36} and which have a correlation length of approximately one CDW period. At lower temperature, the correlations start to grow into larger CDW domains, as evidenced by the increased correlation length. Below this, bulk d -wave superconductivity intervenes at T_{SC} whereupon both the CDW amplitude and the correlation length saturate or start to decrease. The doping dependence reveals an anticorrelation between T_{ξ} of and T_{SC} providing evidence for a non-trivial interaction between the CDW and superconductivity. The CDW intensity disappears in heavily overdoped LSCO25, where the Fermi liquid (FL) normal state is

recovered³³. The red diamonds come from the present study. Pink squares and green circles are data extracted from previous work^{14,15,34,39}.